Extracting Turbulence under Breaking Waves in the Surf Zone

Jun Cheng[1] and Ping Wang[2]

Abstract: Separating turbulence from orbital motion under breaking waves in the surf zone is essential to understanding wave-energy dissipation. In this study, velocity data under monochromatic and random waves in the large-scale sediment-transport facility were analyzed using ensemble averaging (EA), high-pass filtering (HPF) and moving averaging (MA) to extract breaking-induced turbulence. Moving averaging provides a simple method for extracting turbulence from velocity measurements under random breaking waves collected at a reasonably high frequency. Various MA time intervals were examined. Three approaches were used to evaluate the ability of MA to extract turbulence, including (1) testing the ability of MA in extracting turbulence from artificially synthesized signals, (2) comparing turbulence strength of monochromatic wave case using MA and EA, and (3) comparing turbulence strength obtained from MA and Butterworth HPF for the random-wave case. The results indicate that approximately 30–42° phase angle (relative to the peak wave period) MA allows reasonable extraction of turbulence. The turbulence extraction particularly at the wave crest and trough can be improved by adjusting the averaging interval. An adaptive MA with variable averaging time is developed. The MA method is further examined and verified using velocity measurements in the inner surf zone at two sites along the west–central Florida coast. **DOI: 10.1061/(ASCE)WW.1943-5460.0000307.**

Author keywords: Wave breaking–induced turbulence; Moving averaging; Ensemble averaging; Nearshore processes; Physical modeling.

Introduction

Turbulence generated by breaking waves in the surf zone plays a key role in transferring wave energy, momentum, heat, and mass into the water body and bottom sediment. Numerous studies have been conducted to document the effects of breaking wave and turbulence on sediment transport (Wang et al. 2002a, b; Scott et al. 2005). However, separating turbulence from the orbital wave motion is a challenging task. Several techniques have been developed aimed at separating wave and turbulence components of the velocity data. A direct operation of high-pass filtering (HPF) with a determined cutoff frequency may miss low frequency turbulence associated with large-scale eddies. In addition, the cutoff frequency is difficult to determine (Nadaoka et al. 1989). Ensemble averaging (EA) has the advantage of allowing large, low-frequency vortices to be extracted as turbulence, if they are not identically repeated wave to wave (Scott et al. 2005). However, EA is only applicable for monochromatic waves that do not exist in nature. Trowbridge (1998) and Shaw and Trowbridge (2001) developed a commonly used measurement method (Feddersen and Williams 2007; Yoon and Cox 2010) extracting turbulence from the difference between velocities measured from two closely spaced sensors. This method requires two synchronized current meters with carefully designed placement locations. Rodriguez et al. (1999) calculated the theoretical velocity spectrum by transforming the measured water-elevation spectrum through a linear model. The difference between the theoretical velocity spectrum and the measured velocity spectrum is recognized as turbulence. This method cannot be used when waves are strongly nonlinear, such as during breaking.

With the recent development of fast sampling current meters (Puleo et al. 2003, 2012), a more straightforward turbulence-extracting method may be developed. Moving averaging (MA) may be an appropriate technique for extracting turbulence in the surf zone (Longo et al. 2002). The applicability of MA to extract turbulence from oscillatory motion is not well understood. First, the suitable time interval of MA needs to be identified. Another issue is that MA has a limited ability to separate one band of frequency from another (Smith 1997); thus, MA has some inadequacy in separating turbulence and wave. This paper investigates two key issues: (1) what an optimal MA time interval is, and (2) how to improve the limited ability of MA to resolve turbulence. The goal of this study is to examine and improve the MA method in extracting turbulence from complicated oscillatory motions associated with breaking waves.

Description of Laboratory and Field Data for Turbulence Analysis

The large-scale sediment-transport facility (LSTF) is a large-scale three-dimensional (3D) movable bed facility (Fig. 1) with dimensions of 30 m cross-shore, 50 m longshore, and has walls 1.4 m high (Hamilton et al. 2001; Wang et al. 2002a, b; Wang and Kraus 2005). Unidirectional, long-crested monochromic and random waves were generated by four synchronized wave generators oriented at a 10° angle to the shoreline. The fine sand (0.15 mm) beach was approximately 25 cm thick, placed over a planar concrete base, and extended 27 m alongshore and 18 m cross-shore. The water level and 3D current velocities were measured at

[1]Ph.D. Candidate, School of Geosciences, Univ. of South Florida, Tampa, FL 33620 (corresponding author). E-mail: jun@mail.usf.edu

[2]Professor, School of Geosciences, Univ. of South Florida, Tampa, FL 33620. E-mail: pwang@usf.edu

Note. This manuscript was submitted on April 28, 2014; approved on February 23, 2015; published online on May 28, 2015. Discussion period open until October 28, 2015; separate discussions must be submitted for individual papers. This technical note is part of the ***Journal of Waterway, Port, Coastal, and Ocean Engineering***, © ASCE, ISSN 0733-950X/06015003(10)/$25.00.

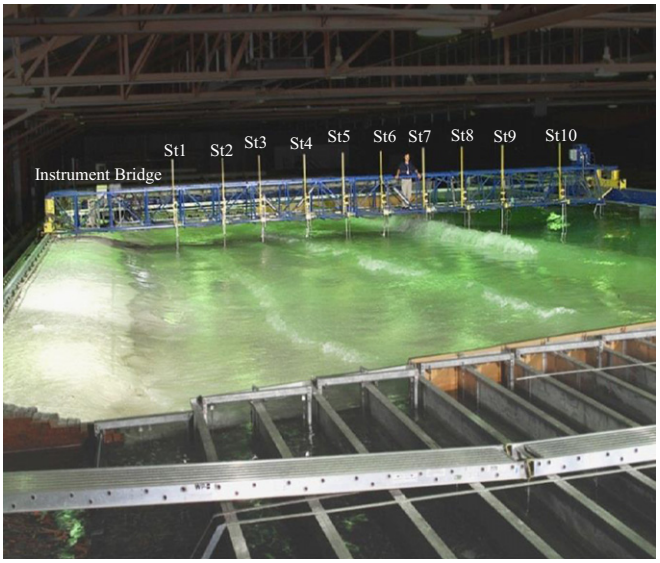

Fig. 1. The LSTF during plunging case, showing the instrument bridge carrying current meters and wave gauges

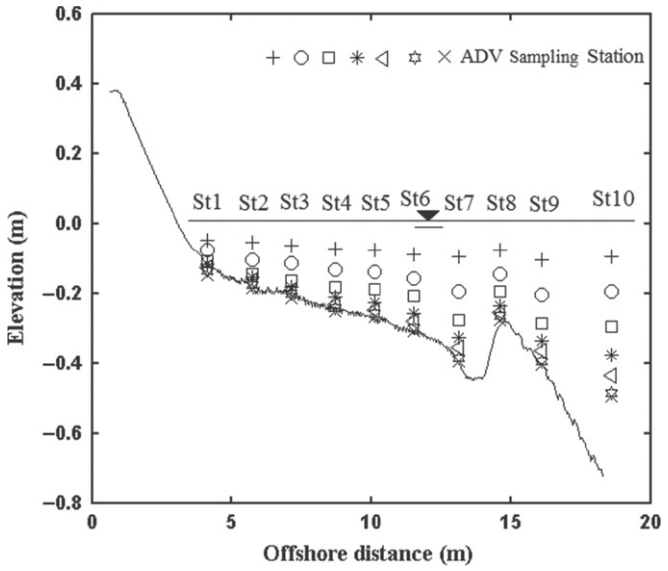

Fig. 2. Cross-shore and vertical measurement locations for the irregular-wave case; the regular-wave case had identical cross-shore measurement locations but only measured at 33% of water depth from the bottom

10 cross-shore locations (Fig. 2) using synchronized capacitance wave gauges and SonTek (San Diego, California) acoustic Doppler velocimeters (ADV) (Kraus et al. 1994), respectively, sampling at 20 Hz. Each sampling event lasted 10 min. The performance and sampling details of the instruments are described in Hamilton et al. (2001) and Hamilton and Ebersole (2001).

Two LSTF cases were examined here: a monochromic wave case with a wave period of 3 s and a random wave case with a peak period of 3 s. The plunging type of wave breaking occurred for both cases (Fig. 1). For the random wave case, the measurements were conducted after the beach had reached equilibrium, i.e., with negligible beach-profile change. For the monochromatic wave case, the measurements were conducted after a 200-min wave action. The beach profile did not reach a stable shape under monochromatic waves (Wang and Kraus 2005). The sampling rate of 20 Hz represents 1/60 of the wave period or peak wave period for the case of random wave (or a 6° phase angle relative to the peak wave period). Measurements conducted in the middle of the test basin are analyzed here. For the monochromic wave case, velocities were measured at roughly 33% of water depth from the bottom. For the random wave case, velocity measurements were conducted throughout the water column from the near bottom up to roughly 80% of water depth from the bottom.

To further verify the method and results from the LSTF, data from two field measurements conducted at the central Gulf coast of Florida examined. The first field experiment was conducted on August 19, 2010, at location N 27°43′58.62″ and W 82°44′57.95″. The local choppy waves of less than 0.5 m in height were mainly generated by typical summer afternoon sea breezes. The second experiment was conducted December 15, 2013, at location N 27°51′15.85″ and W 82°50′47.48″ during the passage of a winter cold front. The incident waves included both distal swells and local choppy waves, with a high of 0.7 m. Several measurements were conducted using a Nortek (Boston, Massachusetts) ADV sampling at a frequency of 64 Hz in the inner surf zone near the secondary breaker line and just seaward of the swash zone. These measurements are used here for the turbulence analyses. As the goal of this study is to test the effect of MA in separating turbulence from wave motion, 5-min sections of velocity data were used here to avoid potential influences of tidal water-level changes on the velocity measurements.

Methodology

Calculating Distribution of Turbulence Kinetic Energy through the Water Column

Spikes sometimes occur in ADV measurements caused by the Doppler signal aliasing and/or air bubbles (Voulgaris and Trowbridge 1998; Longo 2006). A 3D phase space method, originally developed by Goring and Nikora (2002) and validated by Mori et al. (2007), was applied to eliminate the spikes. The removed data points were replaced using cubic polynomial curve fitting.

For the random wave case of the LSTF, Butterworth HPF was applied to the cross-shore velocity. Time-averaged turbulent kinetic energy (TKE) per unit mass ($\overline{k}$) is computed as

$$\overline{k} = \frac{1}{2}(\overline{u'^2} + \overline{v'^2} + \overline{w'^2}) \tag{1}$$

where u', v', and w' = turbulent component in longshore, cross-shore, and vertical direction, respectively.

Examining Various MA Intervals

To examine the applicability of MA on turbulent extraction from the breaking of random waves, the following three tests were implemented. The major parameters applied in these tests are listed in Table 1. The goal of this study is to separate turbulence from wave motion. As the cross-shore velocity has the strongest influence from wave motion, only the cross-shore velocities are examined here. For both random and monochromic wave cases, the MA value, $\overline{v_j}(t)$ of cross-shore velocity, $v(t)$, is calculated as

$$\overline{v}_i(t) = \frac{1}{i}\sum_{k=-(i-1)/2}^{(i-1)/2} v(t+k) \tag{2}$$

where t = time when the velocity was measured, and i = MA time interval. For the LSTF measurement with a peak wave period of

Table 1. Summary of Parameters Used in the Investigation of an Optimum MA Interval

Test	Parameters	Values
1	Wave period	6 s
	σ_1	0.1
	σ_2	0.15
	σ_3	0.2
2	Wave period	3 s
3	Cutoff frequency	1.75 Hz
Field	Cutoff frequency	1.2 Hz

Note: σ_1, σ_2, and σ_3 indicate various standard deviations of the added white noise.

3 s and a sampling frequency of 20 Hz, the MA interval of 3, 5, 7, and 9 points corresponds to 18, 30, 42, and 54° phase angles (relative to the peak wave period), respectively. The turbulence velocity is obtained by subtracting the $\overline{v_j}(t)$ from the raw instantaneous velocity $v(t)$. The turbulent strength (ϕ'_{MA}) defined as the RMS of the turbulent fluctuation is used here to represent the overall magnitude of turbulence extracted from the MA method.

Three tests are conducted to evaluate the effect of MA in extracting turbulence. In Test 1, artificial wave data superimposed with white noise of various standard deviations were analyzed using MA. By comparing the computed turbulence strength with that of the known turbulence, this test provides a validation of the MA method. The artificial random wave is generated by superimposing three sinusoidal waves as

$$Y = y_1 + y_2 + y_3 \tag{3}$$

where y_1, y_2, and y_3 are

$$y_1 = \sin\left(\frac{2\pi}{5.5}t - \frac{\pi}{4}\right) \tag{4}$$

$$y_2 = 2\sin\left(\frac{2\pi}{6}t\right) \tag{5}$$

$$y_3 = \sin\left(\frac{2\pi}{6.5}t + \frac{\pi}{4}\right) \tag{6}$$

A series of white noise, denoted as N_i, is generated as random signals with zero mean and various standard deviation (σ_i) of 0.1, 0.15, and 0.2. These white noises simulate the turbulence strength typically occurring in the surf zone (Ting and Kirby 1995). The composite waves, including the white noises, are sampled at 60 Hz over a 10-min period. Moving averaging with various intervals (18°, 30°, 42°, and 54° phase angles) are applied to the artificial record of $Y + N_i$, which represents random waves superimposed with turbulence. Moving averaging with various intervals are also applied to $y_2 + N_i$, which represents a monochromic wave superimposed with turbulence. To evaluate the effect of MA intervals, the computed turbulence strength (ϕ'_{MA}) was compared with the known input value (σ_i). The closer the ratio ϕ'_{MA}/σ_i is to 1, the better the MA interval is in separating turbulence from wave.

Test 2 compares turbulence extraction from breaking monochromatic waves at the LSTF using the EA and MA methods. Because the EA method is considered a well-defined way of separating wave and turbulent motion for monochromic waves (Ting and Kirby 1996; Longo 2003; Shin and Cox 2006), it is assumed here that the turbulence extracted by EA is valid and can be used as a benchmark to evaluate the effect of the MA method. For monochromic waves, even in the well-controlled laboratory environment, the generated wave periods fluctuate slightly. A modified EA method, a variable interval time-averaging (VITA) method (Longo 2003) was applied:

$$\langle v_{VA}(t)\rangle = \frac{1}{N}\sum_{k=0}^{N-1} v(t + t_K) 0 \le t < \min(T) \tag{7}$$

where $t_k =$ time when the wave crest occurs, and $\min(T)$ was identified as 2.9 s. The turbulence strength obtained from the VITA method was calculated and denoted as ϕ'_{VA}. To avoid possible influence by potential low-frequency oscillation, which sometime occurs during monochromic wave runs in wave basins (Kraus and Smith 1994; Hamilton et al. 2001; Wang and Kraus 2005), a section of 40-s record (or 13 waves) near the beginning of the regular-wave run (0–40 s) was used in the EA. The ratio ϕ'_{MA}/ϕ'_{VA} was used to evaluate the optimum time interval of the simple MA in extracting turbulence from monochromic waves.

Test 3 compares turbulence extraction from breaking random waves using MA and HPF methods. It is assumed here that with a properly selected frequency threshold, the turbulence extracted by HPF can be used as a benchmark to evaluate various time intervals of the MA method. This assumption relies on the large signal-to-noise ratio of the measured velocity to minimize the effect of instrument noise. The magnitude of instrument noise is also examined in this test. The threshold-frequency separating wave and turbulence are determined from the shape of the velocity spectrum, in addition to the limitation of the wave-generation apparatus at the LSTF. The highest-frequency component in the random wave generated at the LSTF is between 1.5 and 2 Hz (Hamilton et al. 2001). Therefore, it is assumed that signals with a frequency higher than 1.75 Hz (the middle point between 1.5 and 2.0 Hz) are not related to the generated waves and, therefore, should be turbulence. The turbulence strength obtained from HPF is denoted as ϕ'_{HP}. Here, ϕ'_{MA}/ϕ'_{HP} is used to evaluate a particular time interval of the MA method in extracting turbulence. Similar methods are also applied to the field data to further examine the applicability of the MA method for extracting turbulence.

Results

Vertical Distribution of Turbulent Kinetic Energy

For the random wave case of the LSTF, the velocities were measured at seven levels (Fig. 2). The vertical distribution of the time-averaged TKE ($\overline{k}$) is examined with the goal of selecting a level with the strongest turbulence to test the applicability of the MA method in extracting turbulence. The HPF method was used here to obtain the turbulent components and subsequently $\overline{k}$ using Eq. (1).

The magnitude of $\overline{k}$ decreased rapidly for nearly one order of magnitude downward within 15 cm from approximately 70% water depth to roughly 50% from the bottom (Fig. 3). The minimum magnitude of $\overline{k}$ occurred at approximately 10–30% of the water depth from the bottom, followed by an increase downward due to the generation of bed-induced turbulence. At St8 over the bar crest (Fig. 2), the $\overline{k}$ values, both near the bottom and near the surface, are generally greater than those at the rest of the cross-shore locations, apparently related to active wave breaking, especially that of larger waves (Fig. 1). A large $\overline{k}$ value near the water surface was also measured at St4, corresponding to secondary wave breaking in the inner surf zone (Figs. 1 and 2). Similar vertical and cross-shore distribution patterns of $\overline{k}$ were measured by Scott et al. (2005) and Yoon and Cox (2010). Because the magnitude of turbulence energy near the water surface is the greatest (based on

the HPF method), the velocities measured near the water surface at 70% of water depth from the bottom were used here to examine the applicability of the MA method for extracting turbulence.

It is beyond the scope of this paper to examine the detailed distribution patterns of $\bar{k}$ in the surf zone. The $\bar{k}$ distribution discussed earlier agrees qualitatively with observations made during laboratory experiments and with existing studies (Scott et al. 2005; Yoon and Cox 2010). This confirms that the LSTF data, in addition to the routine quality control described by Hamilton et al. (2001), are suitable for investigating turbulence extraction.

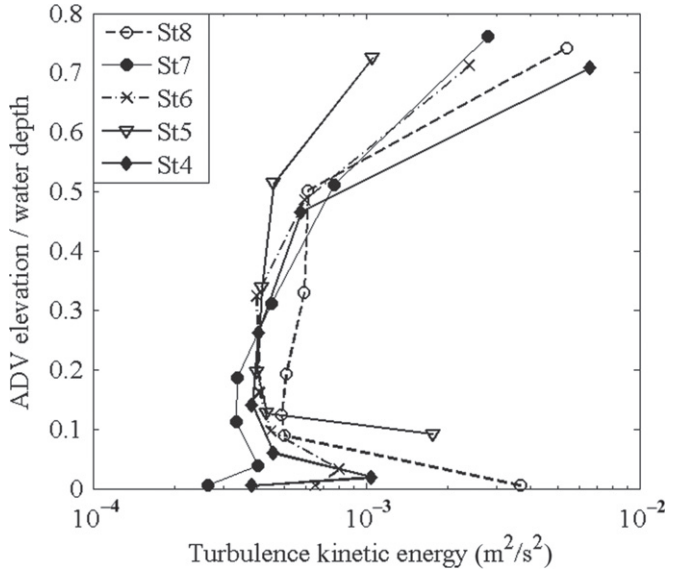

Fig. 3. Turbulent kinetic energy distribution through the water column across the surf zone

Cross-Shore Wave Deformation

For the monochromic wave case of the LSTF, wave breaking was concentrated at St5, as illustrated by the apparent wave deformation [Fig. 4(a)]. As the VITA method uses the interval of peaks in simultaneously measured water level to identify the slight change in periods, the water level is also plotted on Fig. 4(a). The progressive wave deformation is apparent as the wave moves towards the shore. The wave became higher and more asymmetrical from St8 to St6 because of shoaling. The wave height decreased significantly at St4 because of energy dissipation through breaking. The capacitance wave gauges at St5 malfunctioned. The extracted turbulent fluctuation using the EA method is shown in Fig. 5(a). It is worth noting that the velocities for the monochromic wave case were measured at 33% water depth from the bottom, in contrast to the higher 70% water depth for the random wave case. The magnitude of the turbulence fluctuation is not directly comparable because of the different measurement levels.

As apparent from Fig. 4(a), the substantial wave deformation associated with wave breaking at St4 induced a large artificial turbulence velocity computed using the EA method, illustrated by overlying VITA-averaged records over the measured data

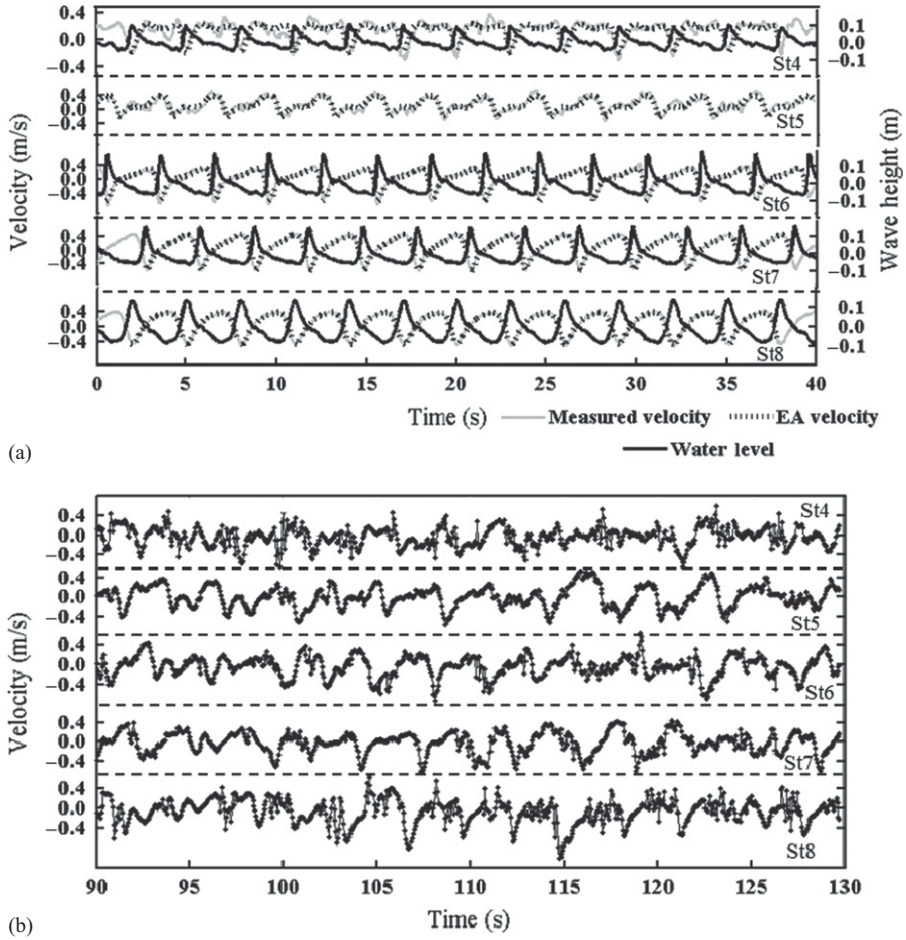

Fig. 4. Examples of measured cross-shore velocity for the (a) monochromatic and (b) random wave case

J. Waterway, Port, Coastal, Ocean Eng.

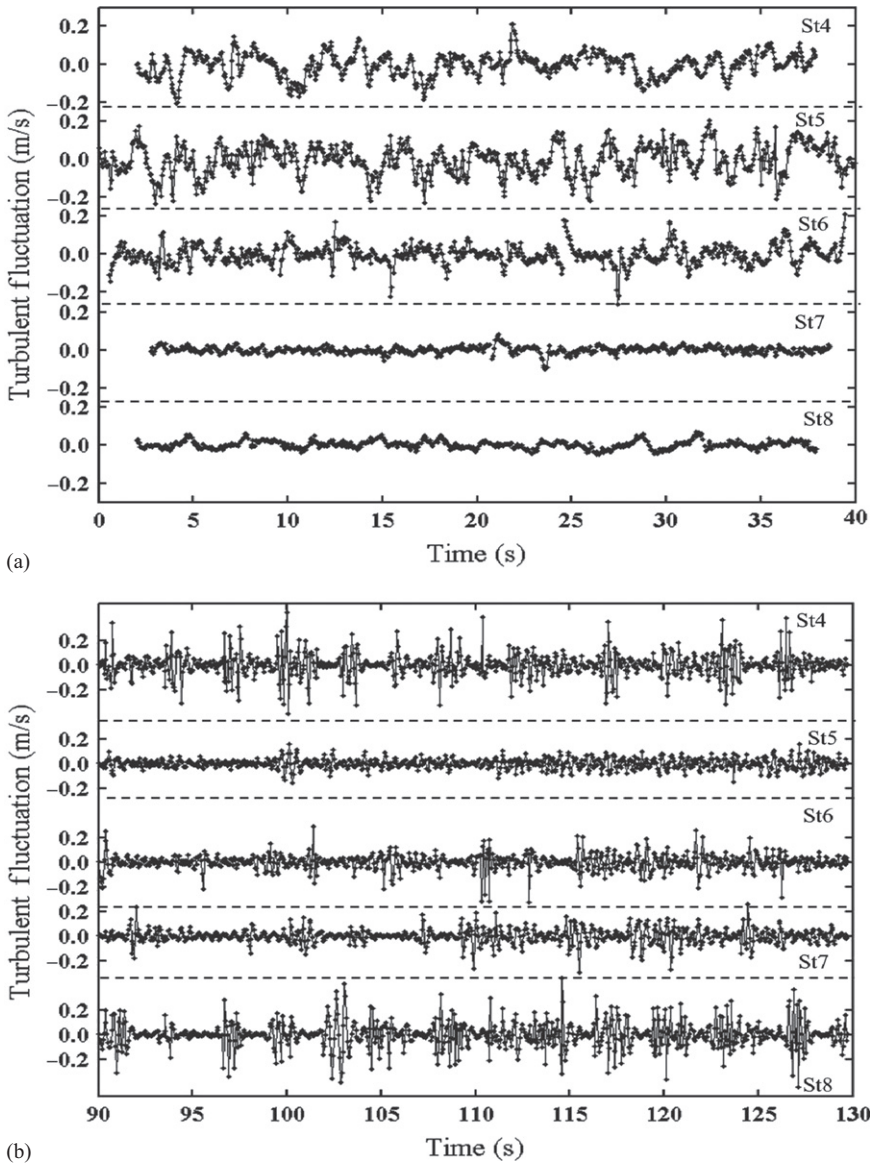

Fig. 5. Turbulence fluctuations extracted from (a) monochromatic and (b) random wave case

[Fig. 4(a)]. Therefore, the large residual (turbulence) velocities at St4 [Fig. 5(a)] resulted from the wave-shape distortion and should not represent turbulence components. Wave shape as measured by the capacitance water-level guages showed considerable wave-to-wave variations in shape, especially under the breaking wave condition [Fig. 4(a)]. For the more realistic random wave case [Fig. 4(b)], the random variations of wave-shape, in addition to the deformation due to breaking, makes EA not applicable.

For the random wave case of the LSTF, turbulence, in the form of rapid velocity variations, is apparent at the wave trough at the main breaker line, especially for large breaking waves [Fig. 5(b), St8]. Directly landward at St7 and St6, considerable turbulence was also measured between crest and trough. The wave form became increasingly deformed further near shore. The spectrum of the measured velocity across the surf zone is illustrated in Fig. 6. It is apparent that the dominant wave period is about 3 s. This peak becomes less dominant as the wave approaches the shore, caused by the transformation of high-frequency motions to low-frequency motions (Butt et al. 2005). Another feature is that the spectrum has a pivot point around 1.75 Hz, coincident with the high-frequency limit of the wave generators, above which the spectral energy

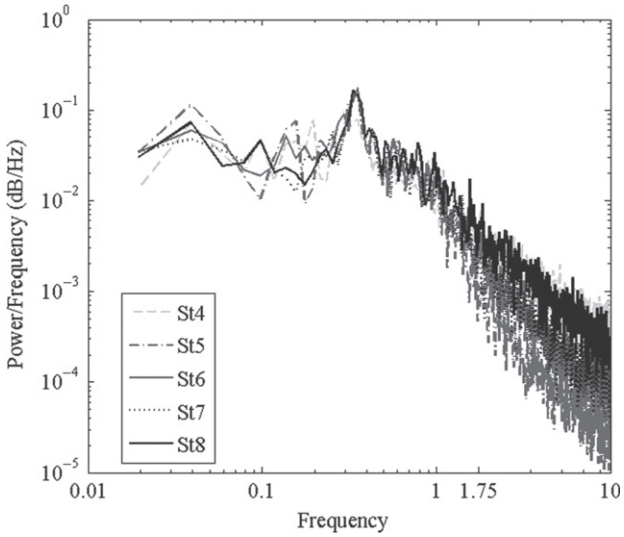

Fig. 6. Spectra of raw velocity measured at several locations across the surf zone in the LSTF

J. Waterway, Port, Coastal, Ocean Eng.

varies significantly among the different cross-shore stations. Thus it is reasonable to use 1.75 Hz as a threshold frequency to extract the turbulence.

Influence of Time Interval on MA

For Test 1 using artificial monochromatic and random waves superimposed by synthetic turbulence, the accuracy of MA was evaluated using a comparison between the computed turbulence strength and the input value in terms of fractions (0.1, 0.15, and 0.2) of standard deviation. Fig. 7(a) indicates that the near unit value of ϕ'_{MA}/σ_i largely occurred between 30° and 42° phase angle MA.

For Test 2 using monochromic wave data from the LSTF, ϕ'_{VA} obtained from the modified EA (VITA) was used as a reference value to examine the empirical application of the simpler MA method. The values of the turbulence strength computed from the modified EA method are listed in Table 2. For the nearshore gauges St4 and St5, the small ϕ'_{MA}/ϕ'_{VA} values [Fig. 7(b)] regardless of the MA interval are likely influenced by the not exactly identical wave deformation, resulting in too-large ϕ'_{VA} values [Figs. 4(a) and 5(a)]. Therefore, the EA method can only be used for measurements outside the surf zone. At St7 and St8, the 42° and 54° phase angle MA generally yielded near-unit values of ϕ'_{MA}/ϕ'_{VA}, respectively [Fig. 7(b)]. Because of the overall weak turbulence at St7 and St8, both the ϕ'_{MA} and ϕ'_{VA} values were small and therefore are more sensitive to small changes (or uncertainties). St6, just seaward of intense wave breaking, should be the most appropriate location for turbulence extraction using EA. The 42° phase angle MA yielded a near-unit value of ϕ'_{MA}/ϕ'_{VA}.

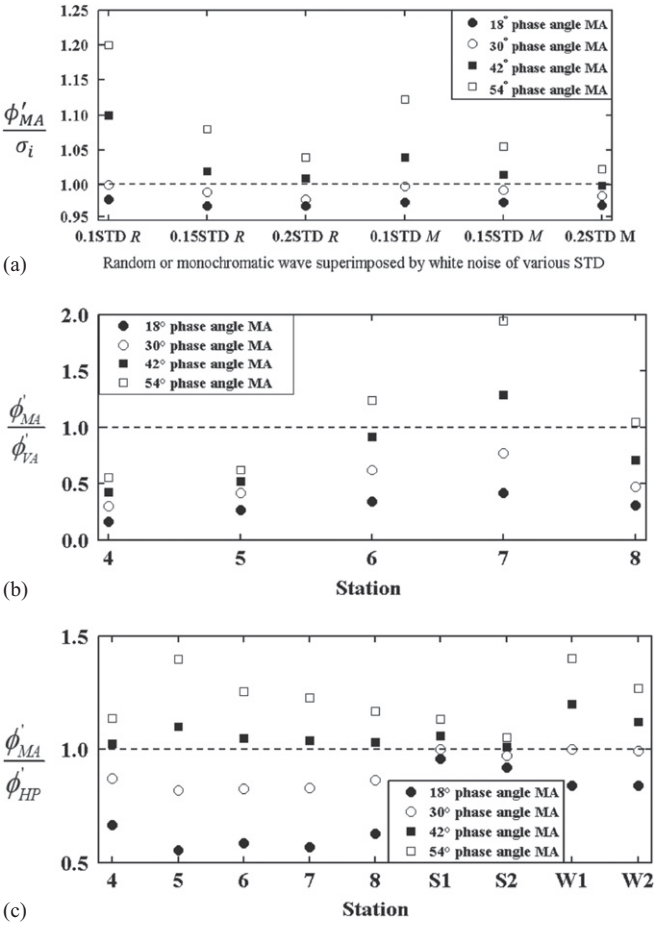

Fig. 7. Comparing turbulence extraction using MA with different average intervals: (a) synthetic signal (*R* stands for regular wave, *M* stands for monochromatic wave) compared with the known value; (b) the LSTF monochromatic waves compared with EA extraction; and (c) the LSTF random waves and field data compared with Butterworth HPF extraction

For Test 3, using random wave data from the LSTF, HPF was used to examine the applicability of the MA method in extracting turbulence. Moving averaging with various averaging time intervals was evaluated by comparing ϕ'_{MA} with ϕ'_{HP}, obtained from the Butterworth HPF, with a cutoff frequency of 1.75 Hz. As the MA time interval increased, the value of ϕ'_{MA}/ϕ'_{HP} also increased, indicating that more wave motions were included by the MA method. The unit value of ϕ'_{MA}/ϕ'_{HP} occurred between 30° and 42° phase angle of MA [Fig. 7(c)]. The values of the turbulence strength computed from HPF are listed in Table 2. The energy above the threshold frequency should include both turbulence and noise. The noise level of the ADV is in the range of ±0.95 to ±3.0 mm/s (Voulgaris and Trowbridge 1998), which is roughly one order of magnitude smaller than the turbulence strength computed in this case (Table 2). Thus, the noise level should not alter the results.

Application of MA to Field Data

Afternoon sea breezes are a major mechanism in generating waves during the typically calm summer season in west–central Florida (Hsu 1988). This is illustrated in an example from the field measurement conducted during the summer of 2010. To examine it closely, the spectrum is plotted in linear scale (Fig. 8). It is apparent that, at noon before the sea breeze strengthened, the peak wave frequency was 0.17 Hz, corresponding to a peak-wave period of 5.8 s, representing small swells coming from offshore S1 in Fig. 8. The example of measured velocity in the cross-shore direction is illustrated in S1 in Fig. 9(a). When the sea breeze strengthened in midafternoon, the wave spectrum evolved into a broad shape with several peaks, including low-frequency swells and high-frequency locally generated waves. The continued growth of the locally generated waves shifted the peak-wave period to approximately 4 s later in the afternoon [Fig. 8(S2)]. The corresponding measured velocity is presented in S2 in Fig. 9(a).

Cold-front passages in the winter are the main driver for energetic conditions along the west–central Florida coast (Wang et al. 2011). Cold-front passages are much larger-scale weather phenomena than summer sea breezes (Hsu 1988). W1 in Fig. 8

Table 2. Turbulence Strength Computed for Monochromic and Random Wave Cases and for Field Data

Station	Turbulence strength (m/s)	
	Monochromic wave (EA)	Random wave (HPF)
4	0.062	0.091
5	0.079	0.036
6	0.050	0.054
7	0.019	0.058
8	0.021	0.090
S1	—	0.056
S2	—	0.077
W1	—	0.082
W2	—	0.071

Note: For the lab data, 4, 5, 6, 7, and 8 indicate the cross-shore locations of measurements. For the field data, (S1) is the example before the full development of sea breezes, (S2) is the example after the full development of sea breezes, (W1) is the example before the passage of a cold front, and (W2) is the example during a cold-front passage.

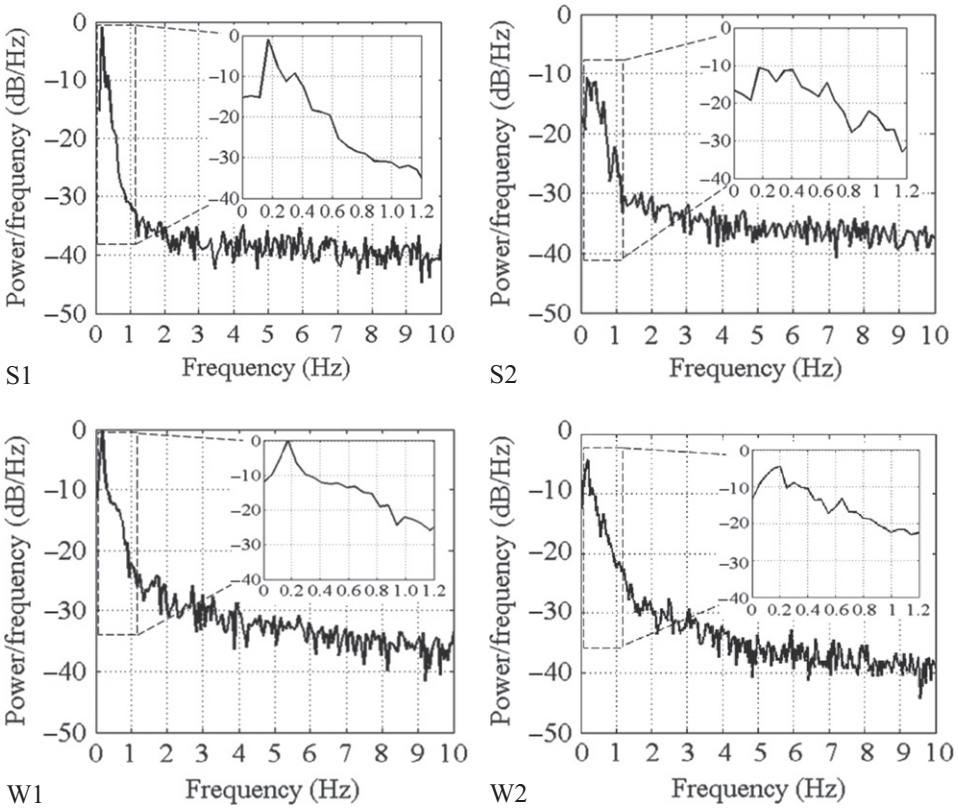

Fig. 8. Velocity spectra of the field data: (S1) example before the full development of sea breezes; (S2) example after the full development of sea breezes; (W1) example before the passage of a cold front; (W2) example during a cold-front passage

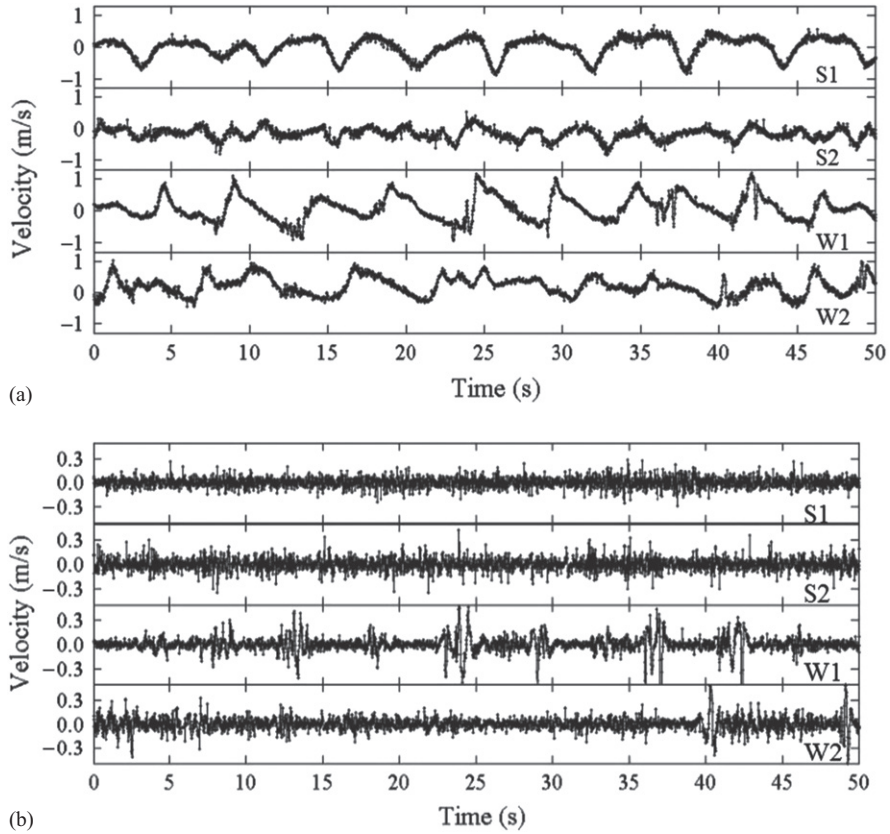

Fig. 9. Examples of (a) the measured instantaneous velocity and (b) the corresponding turbulence fluctuations extracted from Butterworth HPF: (S1) example before the full development of sea breezes; (S2) example after the full development of sea breezes; (W1) example before the passage of a cold front; (W2) example during a cold-front passage

illustrates an example of a prefrontal southerly approaching wave condition. A distinct peak is apparent in the swell-type spectrum of the measured velocity, with peak period approximately 6 s (W1 in Fig. 8). W2 (Fig. 8) shows an example of a northerly approaching wave during the passage of the cold front. The spectrum is relatively broad, with several secondary peaks and a peak-wave period of roughly 5 s. The velocity record associated with the prefrontal and during-frontal spectra are presented in W1 and W2, respectively, in Fig. 9(a).

A distinctive characteristic of these spectra (Fig. 8) is that a pivot point exists at around 1.2 Hz. From the peak frequency to the 1.2-Hz pivot point, spectral density decreases rapidly. In comparison, beyond 1.2 Hz, the spectral density remains relatively stable with a modest range of variations, which likely represents energy from turbulent motion. Therefore, it is assumed that 1.2 Hz can be used here as the cutoff frequency for HPF to separate the wave and turbulence components. The turbulence obtained from HPF with a 1.2-Hz cutoff frequency associated with four examples of measured velocity is illustrated in Fig. 9(b).

Consistent with the MA procedures applied to the LSTF data, 18°, 30°, 42°, and 54° phase angles (relative to the peak wave periods) MA were applied to these four records of the field data, respectively. The value of ϕ'_{MA}/ϕ'_{HP} for these records was computed and is illustrated in Fig. 7(c) together with the laboratory data. The values of the turbulence strength computed from HPF are listed in Table 2. Again, the turbulence strength values are substantially greater than the range of the ADV's noise level (Voulgaris and Trowbridge 1998); thus, the instrument noise should not affect the overall results. On the basis of this field data, the optimum MA interval is between 30° and 42° phase angle.

Discussion

Optimal MA Time Interval

Various datasets are used in the above tests to investigate the capability of MA in turbulence extraction. The test of the artificially generated signals provides a quantitative validation of MA, as the input-turbulence strength is known. The monochromatic and random-wave data collected at the LSTF provides a case under controlled conditions. As the physical model is limited by spatial scale, the generated waves are restricted to short periods. The value of 20 Hz should be considered as the low end of the sampling frequency for turbulence measurement in this case. The field data with longer peak-wave periods sampled at a faster value of 64 Hz provides a supplement to investigate the applicability of the MA method. The overall results suggest that MA with time intervals of approximately 30–42° phase angles provides a simple yet satisfactory empirical method for extracting wave breaking–generated turbulence.

The spectra of the moving-averaged velocities with different averaging intervals at St8 from the LSTF are shown in Fig. 10 in comparison with raw and low-pass filter (LPF) velocities. The moving-averaged velocity led to reduced energy in both wave and turbulence components, and the reduction in both components increased as the MA interval increased, as expected. Averaging over a large phase angle leads to the reduction of wave amplitude. Therefore, it is desirable to average over as small a phase angle as possible, whereas still allow the extraction of turbulence. Here, an adaptive MA is proposed, aiming at minimizing the reduction of wave energy and maximizing the extraction of turbulence (Fig. 11). The procedure of the adaptive MA is illustrated in the following in detail.

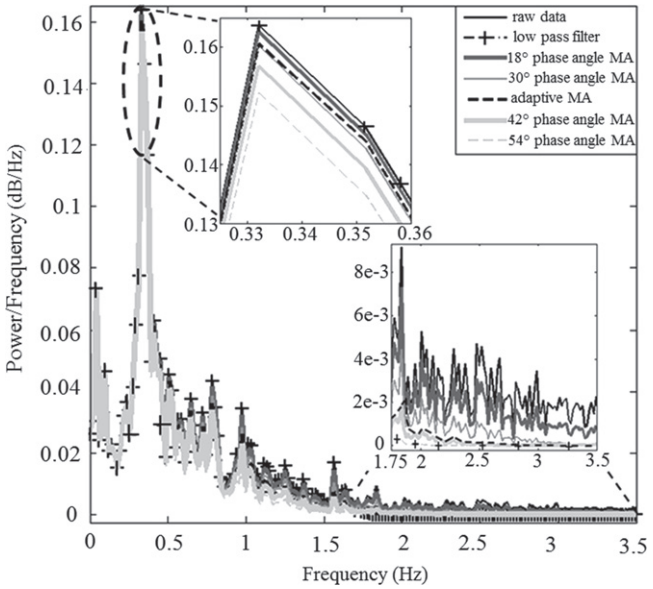

Fig. 10. Comparison of spectra of raw velocity and velocity processed with LPF, MA of various time intervals, as well as the adaptive MA

On the basis of the discussion in the previous sections, 30° and 42° phase angle MA provide fairly accurate extraction of turbulence. The adaptive MA attempts to further improve the simple MA method. The adaptive MA includes two steps. First, a 30° phase angle MA is applied to minimize the reduction of wave energy. As shown in Fig. 11, the 30° phase angle MA failed to extract some turbulent motion, especially at the wave peak and trough, where turbulence tends to be strong. To further extract turbulence, a subsequent 18° phase angle MA is applied to the sections with active turbulent motion (Fig. 11). The sections with active turbulent motion are identified using adjacent local maximum and minimum values. By conducting 18° phase angle MA over these sections, more turbulent fluctuation is resolved, as illustrated in Fig. 11. The localized 18° phase angle MA does not have significant influence on the reduction of wave amplitude. As shown in Fig. 10, the adaptive MA maintains the wave energy comparable to that of 30° phase angle MA, whereas reducing the turbulence energy comparable to the level of 42° phase angle MA.

Advantage and Limitation of the MA Method

The MA method has been widely used in smoothing and removing noise in signal processing (Smith 1997), as well as in extracting turbulence from unidirectional flow (Munson et al. 2006) and various autocorrelated signals (Moncrieff et al. 2004). An apparent advantage of MA is its computational simplicity. From a measurement perspective, MA only requires one sensor with a reasonably fast sampling frequency, making the method applicable for modern fast-sampling technology. Furthermore, the adaptive MA proposed in this study provides a straightforward example demonstrating the capability of MA focusing on velocity variation within a local and changeable temporal window. This implies that the MA method can potentially capture intermittent characteristics of the turbulence velocity.

Turbulence analysis is still an open question. So far, no existing method or model can give an exact value of turbulence, and many possibilities exist for parameterizing turbulence (Puleo et al. 2004). Although EA is widely considered as a benchmark method (Ting and Kirby 1996; Longo 2003; Shin and Cox 2006),

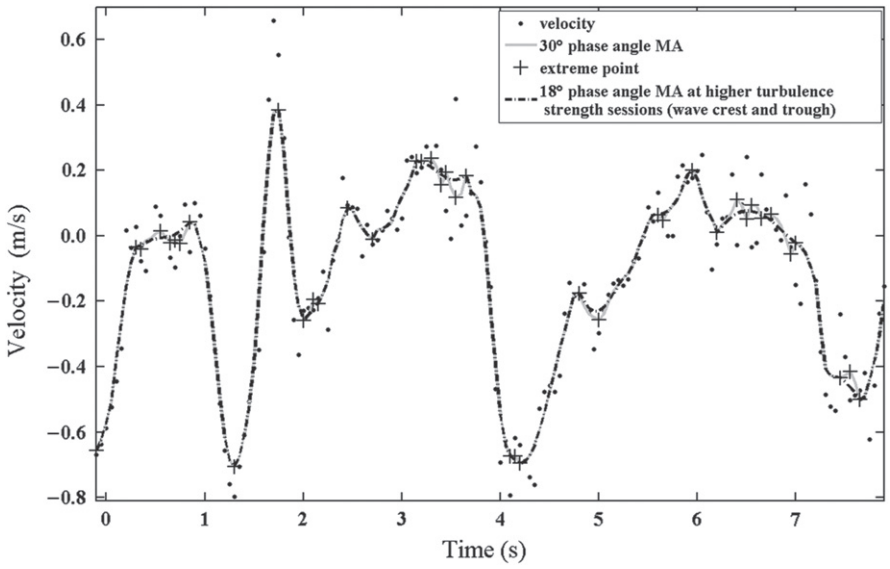

Fig. 11. An example illustrating the adaptive MA with an overall 30° phase angle MA with localized 18° phase angle MA for sections with higher turbulence strength; this method can improve the resolution of turbulence at the crest and trough of the wave

wave deformation and subsequent breaking creates considerable uncertainty, even for the regular waves generated in the laboratory. This is consistent with the finding that estimates of turbulence based on deviations from the ensemble-mean velocity may not be accurate because they would have overestimated turbulence owing to wave deformation (Ogston and Sternberg 2002). For the frequency filtering methods, even if the high cutoff frequency is properly selected, the turbulence velocity in the wave-frequency range and below will be omitted and cause underestimation of turbulence value. Thus, the MA evaluated using these existing methods may contain similar uncertainty. Nevertheless, given the advantage of MA with modern measurement technology, it may shed new light on the turbulence analysis.

Conclusions

The spatial distribution of turbulence generated by breaking waves in the LSTF is examined. The TKE decreased by one order of magnitude downward near the water surface, and reached a minimum value at approximately 10–30% of the water depth from the bottom. The TKE increased further downward because of the generation of bed-induced turbulence. The TKE is substantially greater at the sandbar crest than at adjacent stations. Progressive wave deformation occurred when waves propagated onshore and subsequently broke. Ensemble averaging is not applicable in extracting turbulence motion in the surf zone, even for monochromatic waves because of the substantial wave deformation associated with breaking.

An empirical MA method with various averaging-time intervals was examined to extract turbulence from orbital motion under breaking waves in the surf zone measured both from the LSTF and in the field. Moving averaging with time intervals of approximately 30–42° phase angle provides a simple yet satisfactory empirical method of extracting wave breaking–generated turbulence. Simple MA has a limited ability to separate different frequency bands, such that some turbulence energy failed to be extracted, whereas some wave components were extracted as turbulence. An adaptive MA method was developed to extract turbulence with improved resolution.

Acknowledgments

This study was funded by the Coastal Inlet Research Program of the Army Corps of Engineers and the Challenge Graduate Grant from the University of South Florida. The authors thank Dr. Ernest Smith (USACE) for providing some of the LSTF data.

Notation

The following symbols are used in this paper:

EA = ensemble average;
HPF = high-pass filter;
$\overline{k}$ = time-averaged turbulent kinetic energy (m^2/s^2);
LPF = low-pass filter;
LSTF = large-scale sediment-transport facility;
MA = moving average;
N_i = white noise to simulate turbulence, where i denotes various standard deviations (m/s);
SD = standard deviation;
TKE = turbulent kinetic energy;
VITA = variable interval time averaging;
$\overline{v_j}(t)$ = moving-averaged velocity, where j denotes the time interval of the MA (m/s);
$v_{VA}(t)$ = variable-interval-time-averaged velocity (m/s);
Y = artificial random wave generated by superimposing different regular wave (m/s);
ϕ'_{HP} = turbulence strength computed from high-pass filter method (m/s);
ϕ'_{MA} = turbulence strength computed from moving-average method (m/s); and
ϕ'_{VA} = turbulence strength computed from variable interval time-averaging method (m/s).

References

Butt, T., Russell, P., Puleo, J. A., and Masselink, G. (2005). "The application of Bagnold-type sediment transport models in the swash zone." *J. Coast. Res.*, 21(5), 887–895.

J. Waterway, Port, Coastal, Ocean Eng.

Feddersen, F., and Williams, A. J., III. (2007). "Direct estimation of the Reynolds stress vertical structure in the nearshore." *J. Atmos. Ocean Tech.*, 24, 102–116.
Goring, D. G., and Nikora, V. I. (2002). "Despiking acoustic Doppler velocimeter data." *J. Hydraul. Eng.*, 10.1061/(ASCE)0733-9429(2002)128:1(117), 117–126.
Hamilton, D. G., and Ebersole, B. A. (2001). "Establishing uniform longshore currents in a large-scale sediment transport laboratory facility." *Coastal Eng*, 42(3),199–218.
Hamilton, D. G., Ebersole, B. A., Smith, E. R., and Wang, P. (2001). "Development of a large-scale laboratory facility for sediment transport research." *Tech Rep., ERDC/CHL TR-01-22*, U.S. Army Engineer Waterways Experiment Station, Vicksburg, MS.
Hsu, S. A. (1988). *Coastal meteorology*, Academic Press, San Diego.
Kraus, N. C., Lohrmann, A., and Cabrera, R. (1994). "New acoustic meter for measuring 3D laboratory flows." *J. Hydraul. Eng.*, 10.1061/(ASCE)0733-9429(1994)120:3(406), 406–412.
Kraus, N. C., and Smith, J. M. (1994). "Supertank laboratory data collection project." Volume 1: Main text. *Tech. Rep. CERC-94-3*, U.S. Army Engineer Waterways Experiment Station, Coastal Engineering Research Center, Vicksburg, MS.
Longo, S. (2003). "Turbulence under spilling breakers using discrete wavelets." *Exp. Fluids*, 34(2), 181–191.
Longo, S. (2006). "The effect of air bubbles on ultrasound velocity measurement." *Exp. Fluids*, 41(4), 593–602.
Longo, S., Petti, M., and Losada, I. J. (2002). "Turbulence in the swash and surf zones: A review." *Coastal Eng.*, 45(3–4), 129–147.
Moncrieff, J. B., Clement, R., Finnigan J., and Meyers, T. (2004). "Averaging, detrending and filtering of eddy covariance time series." *Handbook of micrometeorology: A guide for surface flux measurements*, X. Lee, W. J. Massman, and B. E. Law, eds., Kluwer Academic, Dordrecht, Netherlands, 7–31.
Mori, N., Suzuki, T., and Kakuno, S. (2007). "Noise of acoustic Doppler velocimeter data in bubbly flows." *J. Eng. Mech.*, 10.1061/(ASCE)0733-9399(2007)133:1(122),122–125.
Munson, B. R., Young, D. F., and Okiishi, T. H. (2006). *Fundamentals of fluid mechanics*, John Wiley & Sons, New York.
Nadaoka, K., Hino, M., and Koyano, Y. (1989). "Structure of the turbulent flow field under breaking waves in the surf zone." *J. Fluid Mech.*, 204, 359–87.
Ogston, A. S., and Sternberg, R. W. (2002). "Effect of wave breaking on sediment eddy diffusivity, suspended-sediment and longshore sediment flux profiles in the surf zone." *Cont. Shelf Res.*, 22(4), 633–655.
Puleo, J. A., Holland, K. T., Plant, N. G., Slinn, D. N., and Hanes, D. M. (2003). "Fluid acceleration effects on suspended sediment transport in the swash zone." *J. Geophys. Res.*, 108(C11), 3350–3361.
Puleo, J. A., Lanckriet, T. M., and Wang, P. (2012). "Near bed cross-shore velocity profiles, bed shear stress and friction on the foreshore of a microtidal beach." *Coastal. Eng.*, 68(10), 6–16.
Puleo, J. A., Mouraenko, O., and Hanes, D. M. (2004). "One-dimensional wave bottom boundary layer model comparsion: Specific eddy viscosity and turbulence closure models." *J. Waterway, Port, Coastal, Ocean Eng.*, 10.1061/(ASCE)0733-950X(2004)130:6(322), 322–325.
Rodriguez, A., Sanchez-Arcilla, A., Redondo, J. M., and Mosso, C. (1999). "Macroturbulence measurements with electromagnetic and ultrasonic sensors: A comparison under high-turbulent flows." *Exp. Fluids*, 27(1), 31–42.
Scott, C. P., Cox, D. T., Maddux, T. B., and Long, J. W. (2005). "Large-scale laboratory observations of turbulence on a fixed barred beach." *Meas. Sci. Technol.*, 16(10), 1903–1912.
Shaw, W. J., and Trowbridge, J. (2001). "The direct estimation of near bottom turbulent fluxes in the presence of energetic wave motions." *J. Atmos. Ocean Tech.*, 18(9), 1540–1557.
Shin, S., and Cox, D. (2006). "Laboratory observations of inner surf and swash-zone hydrodynamics on a steep slope." *Cont. Shelf Res.*, 26(5), 561–573.
Smith, S. W. (1997). *The scientist and engineer's guide to digital signal processing*, California Technical Publishing, San Diego.
Ting, F. C. K., and Kirby, J. T. (1995). "Dynamics of surf-zone turbulence in a strong plunging breaker." *Coastal Eng.*, 24(3–4), 177–204.
Ting, F. C. K., and Kirby, J. T. (1996). "Dynamics of surf-zone turbulence in a spilling breaker." *Coastal Eng.*, 27(3–4), 131–160.
Trowbridge, J. (1998). "On a technique for measurement of turbulent shear stress in the presence of surface waves." *J. Atmos. Ocean. Tech.*, 15(1), 290–298.
Voulgaris, G., and Trowbridge, J. H. (1998). "Evaluation of the acoustic Doppler velocimeter (ADV) for turbulence measurements." *J. Atmos. Ocean Tech.*, 15(1), 272–289.
Wang, P., Ebersole, B., Smith, R. E., and Johnson, B. D. (2002a). "Temporal and spatial variations of surf-zone currents and suspended sediment concentration." *Coastal Eng.*, 46(3), 175–211.
Wang, P., and Kraus, C. N. (2005). "Beach profile equilibrium and patterns of wave decay and energy dissipation across the surf zone elucidated in a large-scale laboratory experiment." *J. Coastal Res.*, 21(3), 522–534.
Wang, P., Roberts, T. M., Dabees, M., and Horwitz, M. H. (2011). "Beach changes associated with active 2009-2010 El Niño winter along the west–central Florida barrier islands." *Proc., Coastal Sediments 2011*, Vol. 2, World Scientific, Singapore, 1229–1242.
Wang, P., Smith, E. R., and Ebersole, B. A. (2002b). "Large-scale laboratory measurements of longshore sediment transport under spilling and plunging breakers." *J. Coastal Res.*, 18(1), 118–135.
Yoon, H. D., and Cox, D. T. (2010). "Large-scale laboratory observations of wave breaking turbulence over an evolving beach." *J. Geophys. Res.*, 115, C10007.

J. Waterway, Port, Coastal, Ocean Eng.